

Electronic-nose for detecting environmental pollutants: signal processing and analog front-end design

Hyuntae Kim · Bharatan Konnanath · Prasanna Sattigeri · Joseph Wang · Ashok Mulchandani · Nosang Myung · Marc A. Deshusses · Andreas Spanias · Bertan Bakkaloglu

Received: 24 November 2010 / Revised: 18 February 2011 / Accepted: 24 March 2011 / Published online: 11 April 2011
© Springer Science+Business Media, LLC 2011

Abstract Environmental monitoring relies on compact, portable sensor systems capable of detecting pollutants in real-time. An integrated chemical sensor array system is developed for detection and identification of environmental pollutants in diesel and gasoline exhaust fumes. The system consists of a low noise floor analog front-end (AFE) followed by a signal processing stage. In this paper, we present techniques to detect, digitize, denoise and classify a certain set of analytes. The proposed AFE reads out the output of eight conductometric sensors and eight amperometric electrochemical sensors and achieves 91 dB SNR at 23.4 mW quiescent power consumption for all channels. We demonstrate signal denoising using a discrete wavelet transform based technique. Appropriate features are extracted from sensor data, and pattern classification methods are used to identify the analytes. Several existing pattern classification algorithms are used for analyte detection and the comparative results are presented.

Keywords Electronic nose · Gas sensors · Analog front end · ADC · Chopper stabilization · Feature extraction

H. Kim (✉) · B. Konnanath · P. Sattigeri · A. Spanias · B. Bakkaloglu
Arizona State University, Tempe, AZ 85287, USA
e-mail: hkim44@asu.edu; hyuntae.kim@asu.edu

J. Wang
University of California-San Diego, San Diego, CA 92093, USA

A. Mulchandani · N. Myung
University of California-Riverside, Riverside, CA 92501, USA

M. A. Deshusses
Duke University, Durham, NC 27708, USA

1 Introduction

Diesel and gasoline internal combustion engines produce exhaust, which is a complex mixture of gases and fine particles. Several previous studies have linked respiratory diseases and cancer to exposure to gasoline and diesel exhaust [1–4].

National Institutes of Health (NIH) launched an initiative for exploring the environmental roots of these diseases [5]. A reliable and reproducible quantitative measure of exposure is required to establish a direct linkage of these diseases to diesel and/or gasoline exhaust. Traditionally the detection of environmental emissions has been performed by using analytical instruments such as gas chromatography/mass spectrometry (GC/MS) that are expensive, have high operating costs and require trained personnel [6]. These techniques are not appropriate for real-time on-site operation. Electronic noses (e-noses), which rely on arrays of partially-selective chemical sensors for detection of volatile chemicals, are a portable and cost-effective alternative [7]. In the past, e-noses have been used in diverse applications such as spoilage detection of foodstuffs [8, 9], disease diagnosis [10, 11] and process control [12]. Environmental monitoring has become an important area of application of e-noses during the past two decades due to the increasing awareness of the effects of pollution on human health and the quality of the environment [13]. Previously, electronic noses have been used for environmental monitoring in applications such as detection of smoke compounds [14], the determination of indoor air quality [15] and odor emission rate of a compost hall [16]. However they have not been applied for real-time exhaust monitoring problem. Monitoring a large number of pollutant gases and particulates in the air is an emerging application where the potential of the electronic nose is yet

to be established. The introduction of the electronic nose for this task is very challenging. In addition to very complex target mixtures and low detection thresholds, varying ambient conditions such as temperature and humidity distort the analyte signatures [13]. Thus, the classification method must be robust to changes in analyte concentration levels and environmental factors such as temperature and humidity. A mobile sensor system is being developed [17, 18] which is designed to be capable of monitoring up to 40 analytes in diesel and gasoline exhaust in real-time. The system is light-weight and low-cost and can be worn as a badge, similar to a radiation counter.

These light-weight badges will each house an array of electrochemical nanosensors for detecting and measuring trace analytes in exhaust gases. This is in contrast to the current analytical techniques which are expensive, bulky and have significant power requirements. The system consists of:

- an array of partially selective conductometric and amperometric sensors which perform chemical sensing,
- an integrated microelectronic component for power management and data collection (i.e. the analog front-end)
- a signal processing module for automatic identification of the pollutants.

A block diagram of the system is illustrated in Fig. 1 and its prototype badge style sensor platform is shown in Fig. 2. A reconfigurable analog front-end (AFE) sensor interface circuit provides data acquisition and interfaces to the DSP microcontroller. The electrochemical micro-electronics supports a multi-channel electrochemical array with high performance amperometric and conductometric sensors. This sensor front-end consists of

- low noise, programmable readout-amplifiers,
- sensor stimuli DAC and

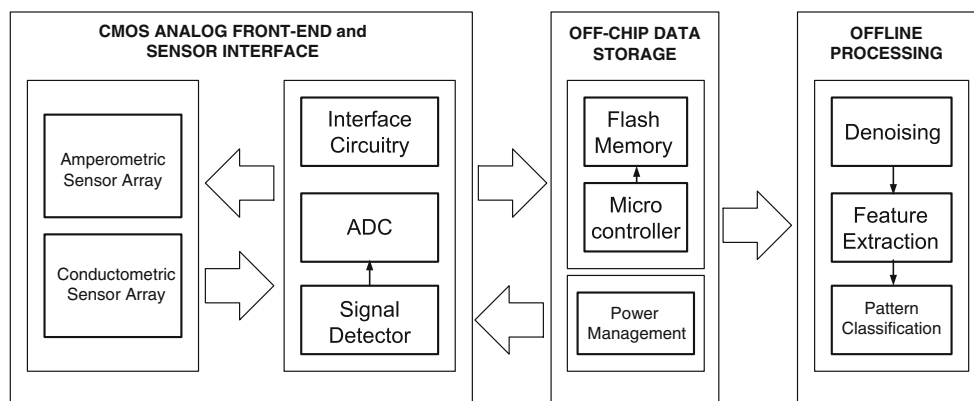


Fig. 1 Block diagram of the proposed exhaust monitoring system

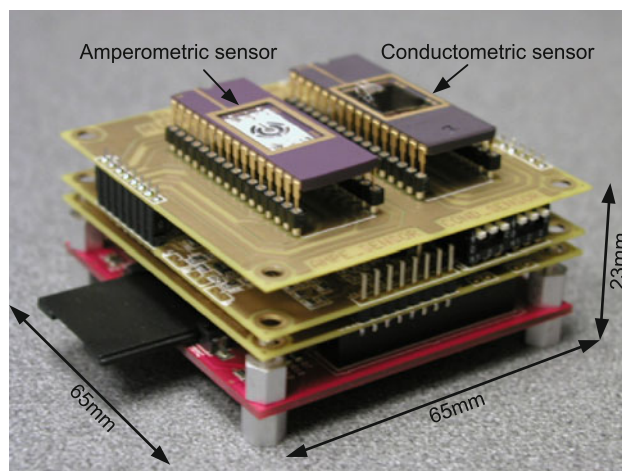


Fig. 2 Proposed badge style sensor platform module

- data conversion circuits.

The surface of the chip provides a CE (counter electrode), RE (reference electrode) and eight WE (working electrode) array for amperometric sensors. Also, the chip provides gate voltage and current sweeping for eight FET based conductometric sensors.

After sensor data acquisition, the next steps in the signal processing stage are denoising, feature extraction and classification for which we have developed and implemented customized algorithms. These algorithms have been evaluated using data from two distinct real-life scenarios, namely;

- The sensors are exposed to a pollutant (usually present in high concentration) for a long period of time, and as a result the sensors saturate and the outputs have a steady-state value.
- The sensors are exposed to a pollutant gas for a short period due to which we obtain a transient response consisting of peaks in the sensor output.

Appropriate combinations of features and classification algorithms for each scenario have been tested offline using Matlab.

The rest of the paper is organized as follows. Section 2 presents the details of the analog front-end. Section 3 describes the denoising approach. The feature extraction and classification techniques as well as the results obtained on synthetic and experimental datasets are detailed in Sects. 4 and 5 respectively. The last Sect. 6 presents concluding remarks.

2 Analog front-end design

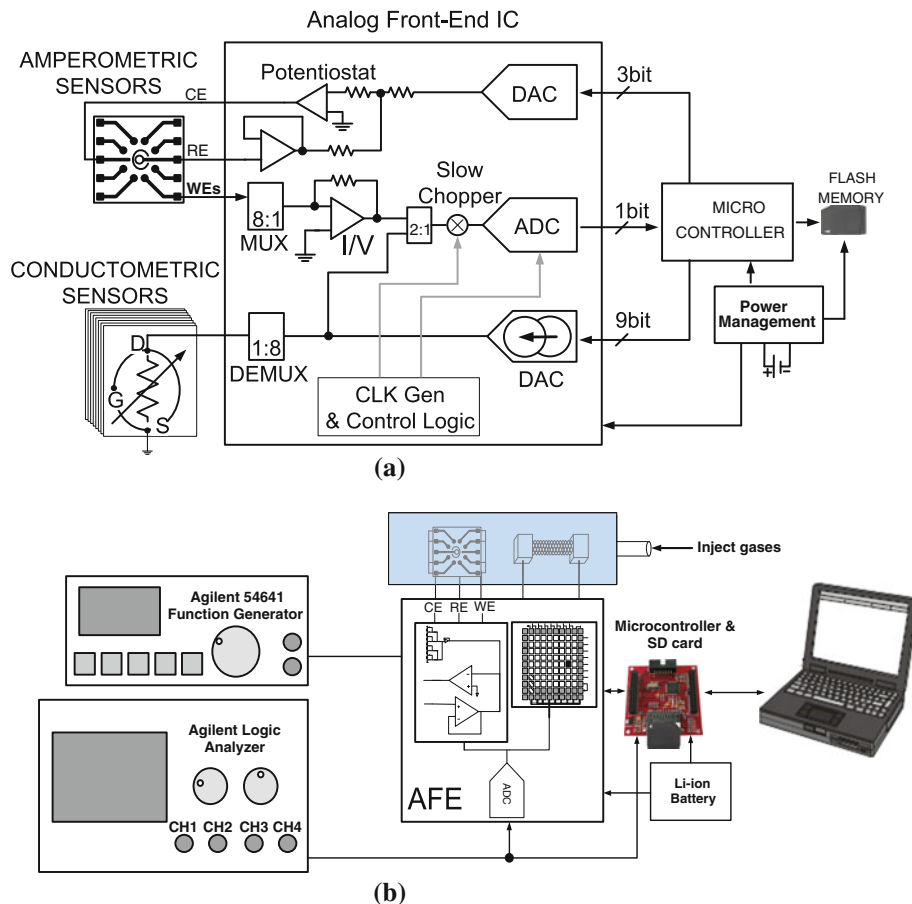
To satisfy the size and power consumption requirements of the measurement system, an integrated readout IC, data acquisition and data signal processing module are required. The signal chain for the readout system is illustrated in Fig. 3(a). Figure 3(b) shows typical measurement setup for analog front-end (AFE) with both conductometric and amperometric sensors. In a typical test application the vapor to be tested is injected into the small chamber and AFE delivers the electrical signals from chemical reaction with gas sensors. The AFE consists of a potentiostat, a current-to-

voltage converter, a resistor string digital-to-analog converter (DAC) and a nested chopped analog-to-digital converter (ADC) for the amperometric sensor as shown in Fig. 4. The gas sensor interface circuitry is made of a current steering DAC, a resistor string DAC for sensor stimuli, and a nested chopped low-offset ADC for the conductometric sensor in Fig. 6. The whole system operates with a supply voltage of 1.8 V and is implemented in 0.18 μm CMOS process with one poly and six layers of metal.

2.1 Amperometric sensor AFE: system implementation

The amperometric sensor produces current output depending on gas concentration while the AFE applies a voltage between working electrodes (WEs) and reference electrode (RE). The applied voltage stimulus can determine sensing mode in amperometric sensor system such as pulse voltammetry or a cyclic voltammetry. In Fig. 4, a three bit resistor string DAC is used as a stimulus for staircase voltammetry. Stimuli sets the potential applied across the electrochemical cell and can be either constant voltage or cyclic voltammetry measurement [19, 20, 44]. Based on sensor response characterization, a 125 mV DC stair step stimulus is generated to get reduction/oxidation between the

Fig. 3 Diagram and bench characterization setup of exhaust gas detection AFE. **a** Block diagram. **b** Test setup



Reference Electrode (RE) and the selected Working Electrode (WE), sweeping from -125 to 870 mV differential signal with respect to a reference electrode (RE) absolute potential of 1 V. However, the approach with DC constant voltage causes only oxidation of electrochemical gases to detect chemical reactions more rapidly. The potentiostat enforces a controlled potential at an electrode to produce the desired perturbation for measuring and recording current versus time response [48]. In Fig. 4, the potentiostat consist of analog devices constructed with operational amplifiers and is used to maintain the voltage between the WEs and the RE. Based on the force to break equilibrium for oxidation/reduction reaction, the Faradaic chemical reaction occurs at the WE. The RE, which ideally carries zero current, and it can track the applied voltage. When a potential is applied to two electrodes (RE and WE) system, the Faradic current from electrode chemical cell is measured as a function of the potential. Since the reference electrode carries sensor biasing current, the electrode will polarize and an over potential will occur. Therefore, the potential at the WE is unknown. To avoid this phenomenon, a three electrode system is used. To satisfy this, a large gain is required for amplifiers A1 and A2 in Fig. 4 [21, 45]. The range of the sensor output signal can occur at an uncertain value within the range of supply voltage. Therefore, the operational

amplifiers should have as high of a signal swing as possible. To achieve high swing, the operational amplifiers should have rail-to-rail outputs and the operational amplifiers should drive the large double layer capacitor of the CE and WE. Also, The Faradaic current based on chemical reaction is amplified by a standard transimpedance amplifier with a feedback resistor, R_f . The SNR of the system at the output of the transimpedance amplifier is given for Fig. 4(b). The SNR of the system at the output of the transimpedance amplifier is given by $SNR = (R_f^2 \circ i_f^2) / (V_{noise,out}^2 + R_f^2 \circ i_{sensor}^2 + kT/C_s)$, where I_f is the faradaic current, $V_{noise,out}$ includes the output offset noise of amp and thermal noise of R_f , i_{sensor} is sensor noise, and kT/C_s represents ADC sampling stage. Based on these requirements, the operational amplifiers are implemented using a rail to rail input stage architecture as shown in Fig. 5 [20]. In fact, the high impedance amplifier at RE ensures that very little current flows through the RE and enforces all current to flow from the CE to the WE when maintaining a constant voltage at equilibrium. The current from the potentiostat is converted to voltage through an I-to-V converter at the input of the ADC. A current range of 10 nA– 100 μ A is detected depending on gas concentration.

Fig. 4 Sensor analog front-end circuit and noise for an amperometric sensor. **a** Interface circuitry for amperometric sensor. **b** Model of a typical readout circuit for amperometric sensor

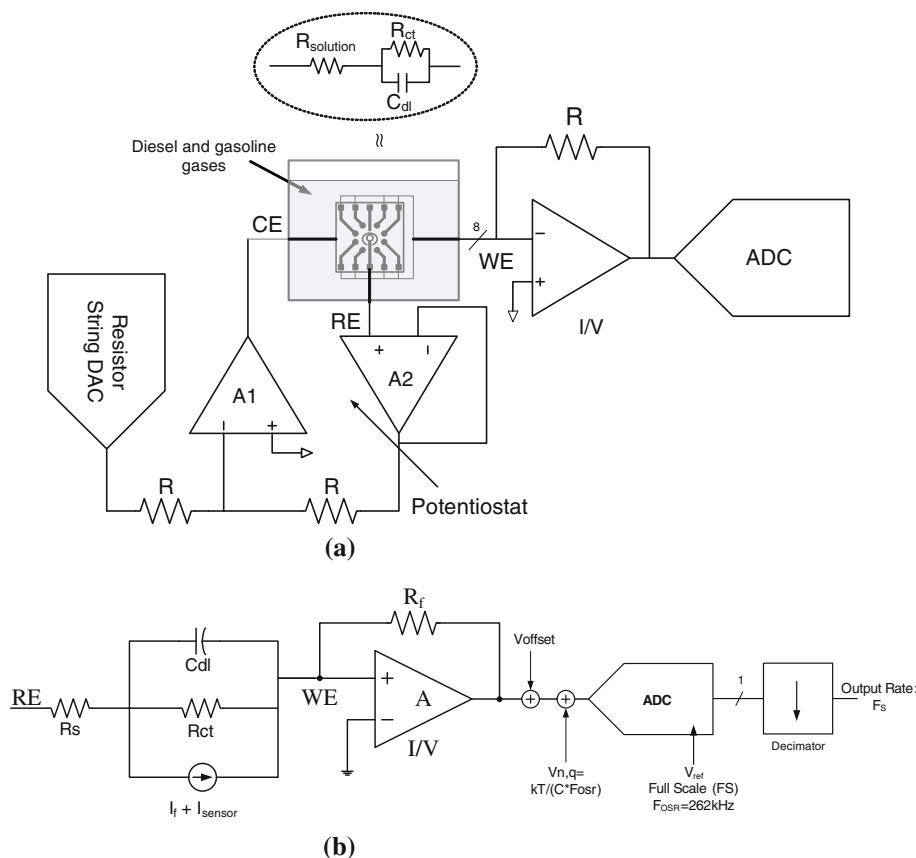


Fig. 5 The single ended rail-to-rail class AB opamp used in the sensor readout front-end

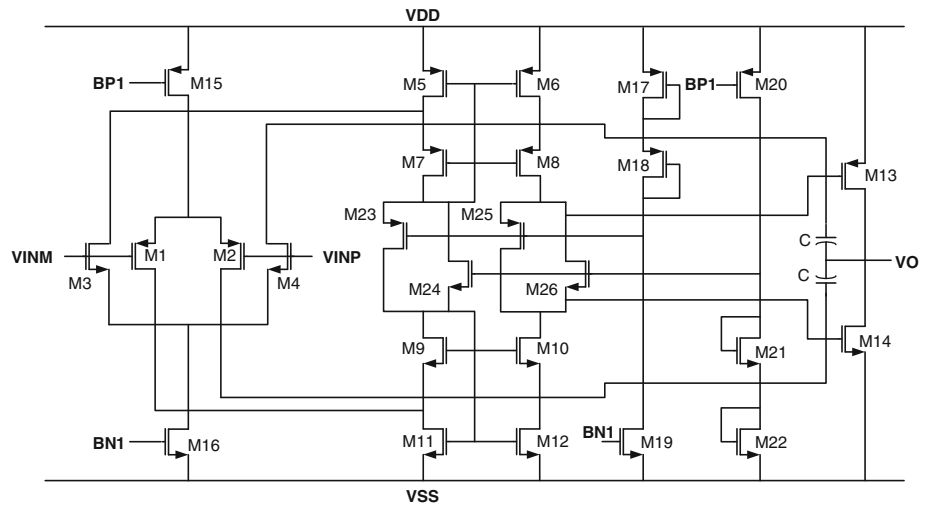
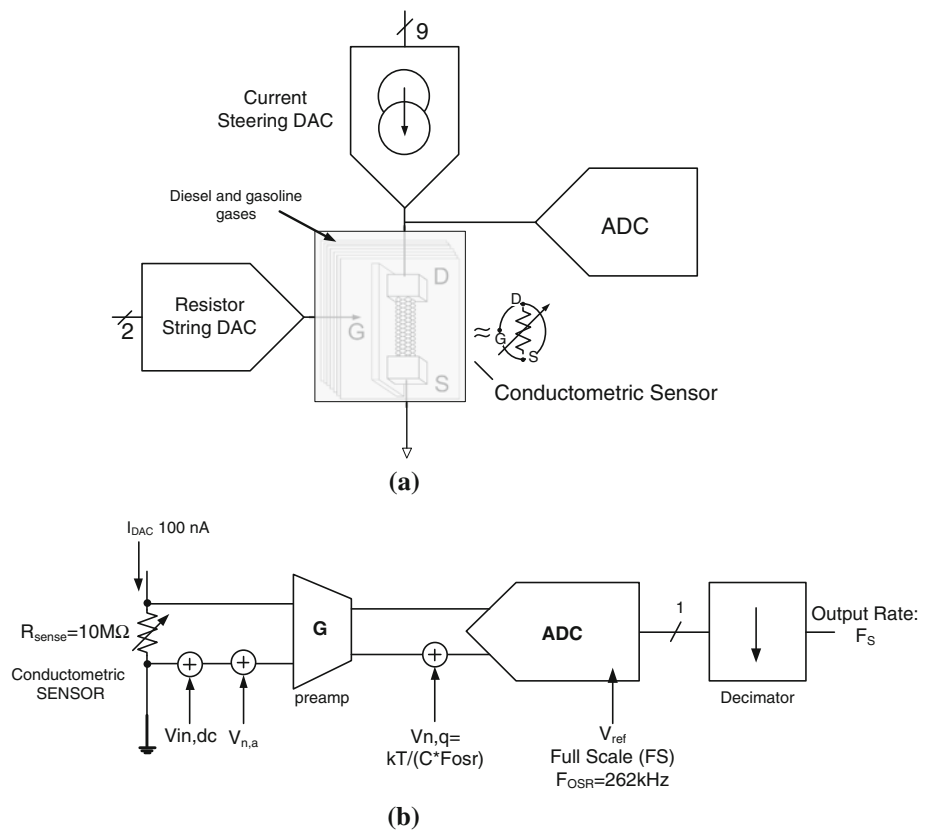


Fig. 6 Sensor analog front-end circuit setup for a conductometric sensor. **a** Interface circuitry for conductometric sensor. **b** Model of a typical readout circuit for conductometric sensor



2.2 Conductometric sensor: system implementation

The conductometric sensor based on single wall carbon nanotube (SWNT) is a miniature three-electrode device designed to measure the conductivity of the gas sensitive nanostructures placed between the electrodes [22]. Figure 6(a) shows the relevant Analog-Front-End (AFE) components for the conductometric sensor. As shown in Fig. 6(b), the noise specification for the ADC. Where $V_{in,dc}$ is input referred offset of preamp, $V_{n,a}$ is preamp input

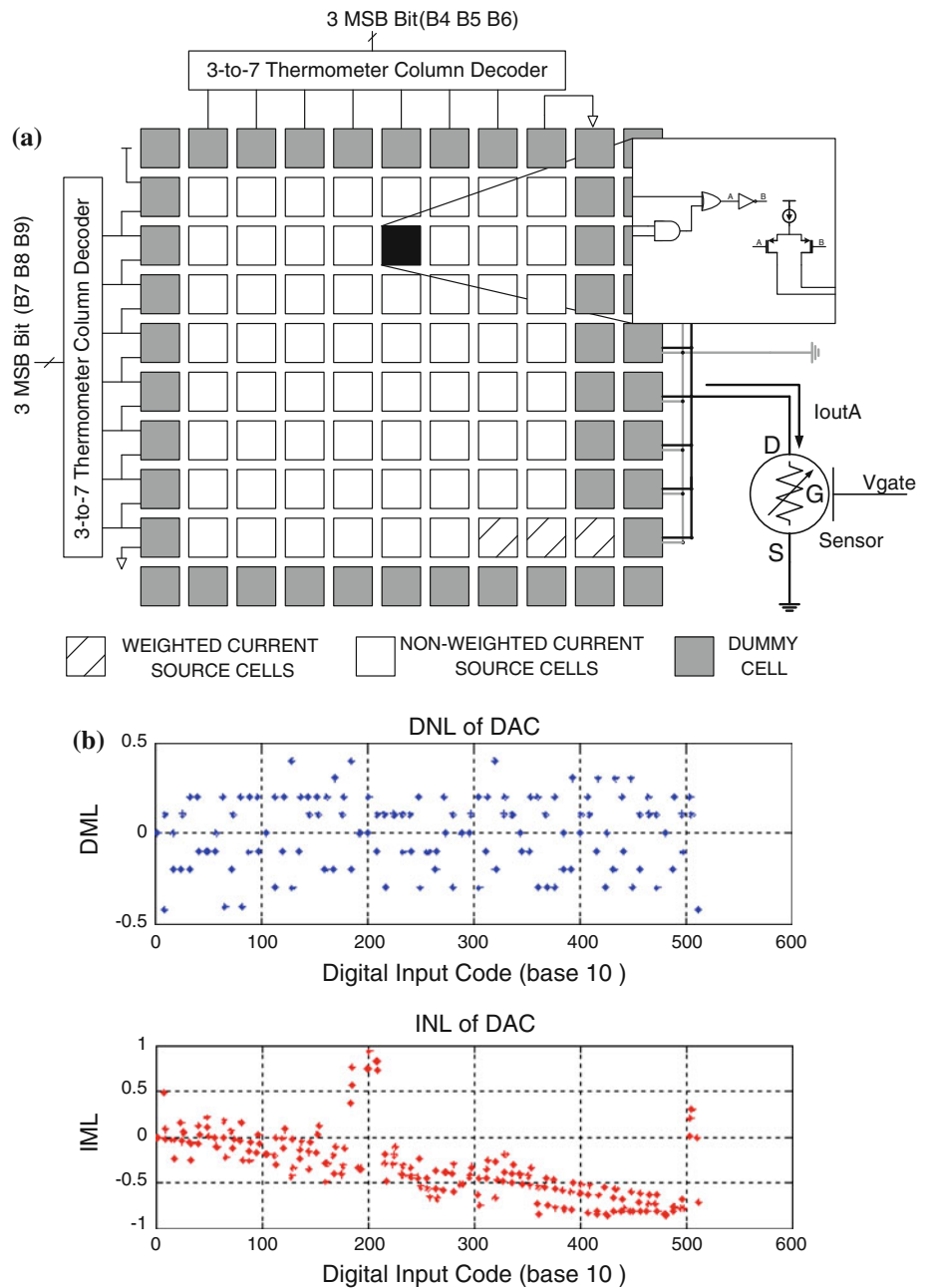
noise, and $V_{n,q}$ is the power spectral density of the quantization noise. Sensing resistor is 10 MΩ and predetermined current source is 100 nA. Input referred noise of resistor is $4kTR$ V²/Hz and preamp noise is typically 3 nV/√Hz. The accumulated output noise at ADC input is about $4kTR$. The noise of ADC is $kT/(Cs*fosr)$. Output signal Total output noise density is $4kTR + kT/(Cs*fosr) + V_{in,dc} + V_{n,a}$.

To precisely measure the large conductance change of the sensor depending on the concentration, a high accuracy

9-bit current steering DAC in Fig. 7(a) is used to push a programmable current level into the sensor array. The current range of the DAC is from 100 nA (equivalent to 1 LSB) to 51.1 μ A. The DAC has a measured DNL of +0.402/−0.42 LSB and INL of +0.941/−0.808 LSB. In order to detect the resistance change in the conductometric sensor with 1% or better accuracy, the sensor stimuli quantization noise should be lower than 1%, which sets the absolute minimum quantization error to be 7 bits. The range of the base resistance in the conductometric sensor is between 10 and 10 M Ω , which covers a 10 bit range. The minimum current from the current steering DAC is

determined by the largest sensor base resistance to measure, as well as the voltage headroom for the current array. In fact, 0.8 V headroom for a cascode current source is required for a 1.8 V supply operation. To measure 10 M Ω with 1.0 V voltage swing at the ADC input, 100 nA is selected as 1 LSB of the DAC. To measure 100 Ω as 1% change in 10 k Ω at 1 V, the maximum current source needed is calculated as 100 μ A. However, carbon nano tube based conductometric sensor can withstand up to 60 μ A only due to reliability limitation. Therefore a 9 bit current steering DAC (51.1 μ A peak current) is chosen. The specific selected current level depends on ADC output

Fig. 7 Implementation and DNL/INL of current steering DAC for the conductometric sensor



code levels and it is controlled by the microcontroller. To increase the conductometric sensor sensitivity level to detect resistance changes when exposed to diesel and gasoline exhaust, a 2-bit R-string DAC with a voltage buffer (Class AB) is used to apply a static voltage to the gate of the sensor. The output of the DAC is used to apply a static voltage to the back-gate of the conductometric sensor. After driving the programmable current to drain and applying voltage to gate of the sensor, the result of the conductance change between drain and source is digitized by $\Sigma\Delta$ ADC.

2.3 First order $\Sigma\Delta$ ADC with nested chopper stabilization

The $\Sigma\Delta$ ADC is used to digitize the electrochemical response voltage which is obtained from the amperometric sensor and the conductometric sensor. The complete signal flow diagram for the ADC with cascaded integrate comb (CIC) decimation filters are shown in Fig. 8(a) [47]. The outputs of both amperometric sensors and conductometric sensors are applied to the same ADC via an analog multiplexer. Two nested choppers modulate the output signal from the sensors to two distinct frequencies. First is a low frequency chopper at the ADC input and the second one has a high frequency inside of the ADC. Figure 8(b) and (c) show the frequency spectrum for nodes W, X, Y, and Z in Fig. 8(a). Figure 8(d) shows the implementation of nested chopper stabilization technique and digital decimation filter with down sampling rate K and M.

The slow chopper is applied to decrease the mismatch related residual offsets in the sampling network and moves the sensor signal to a low chopping frequency [23, 24]. After the external slow chopper modulates the input signal, the first order ADC digitizes the signal at the slow chopper frequency and any potential residual offset at DC at node W as shown in Fig. 8(a). It is critical to keep the slow chopped signal within the flat-band of the quantization noise for the ADC as shown in Fig. 8(b). Inner fast chopper pair is required for pushing $1/f$ noise and DC offset of the ADC integrator to a higher frequency. The high frequency chopping is closed within the integrator, and the digitized signal at the ADC output stays at the lower chopping frequency. The demodulation of the input signal occurs after the first digital low pass filter. The cutoff frequency of the first set of CIC filter should be higher than the chopper frequency to eliminate the risk of high frequency noise demodulation. In fact, the first filter should pass the odd harmonics of signal at odd chopper frequencies because the signal should be reconstructed with low distortion. After the digital demodulator with slow chopper frequency, the signal at the slow chopper frequency is down-converted back to DC by the chopper switches in the digital filter module. Finally, the low frequency drift at slow chopper frequency are eliminated by the second digital low-pass filter as shown in Fig. 8(c) and (d).

A 16 bit converter is targeted for this system, since the system was anticipated to have about 100 dB dynamic range based on sensor noise floor and readout chain gain requirements. The noise floor of the sensor is determined by the sensor electrode size, eventually determining the overall signal chain gain and resolution requirement. For the conductometric sensors used, minimum detectable resistance was determined to be 100 Ω with a 10 k Ω base resistance. This corresponds to a minimum ADC resolution of 10 bits when both amperometric and conductometric sensors are used simultaneously in the gas detection system. The required resolution of sigma delta ADC is between 10 bit and 16 bit, making it flexible for various minimum detection current values and sensor resistances. Output of the ADC is single-bit bitstream data and is stored into flash memory in the gas detection system and post-processed off-line on a PC platform.

The first-order nested chopped $\Sigma\Delta$ modulator architecture is shown in Fig. 9. The first order $\Sigma\Delta$ ADC consists of an integrating amplifier with a 12 pF sampling capacitor according based on kT/C noise requirements, and the ADC operates at 262.144 kHz. The main drawback of the first order $\Sigma\Delta$ ADC is generation of tones and pattern noise due to static frequency content at the input. To reduce tonal behavior and pattern noise, a non-periodic dither signal is applied at the quantizer input. A linear feedback shift register (LFSR) is used to generate a dither signal as shown

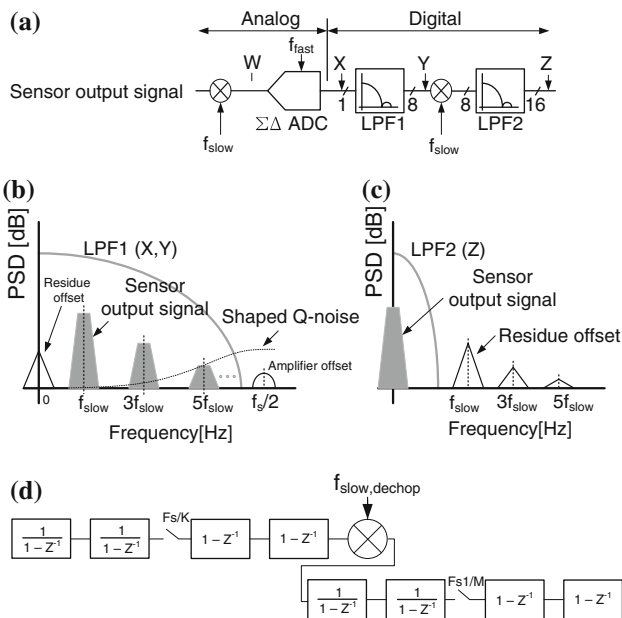
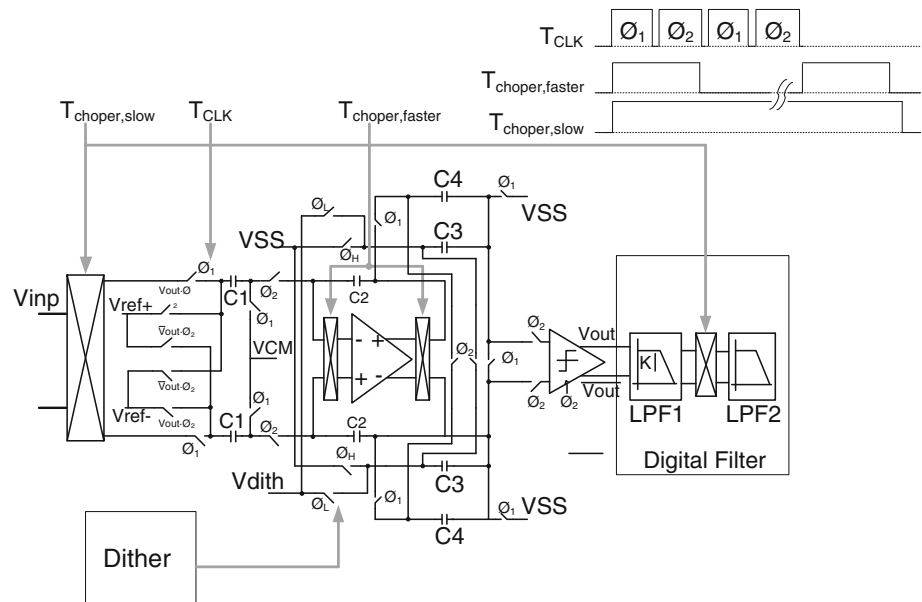


Fig. 8 The complete signal flow diagram and frequency spectrum for $\Sigma\Delta$ ADC with decimation filters

Fig. 9 First order $\Sigma\Delta$ ADC with chopper switches and dither circuit



in Fig. 9 [24, 46]. Figure 10 shows the PSD of the ADC output for a full scale input of 1.2 V. The modulator is operated at a frequency of 262.144 kHz, which yields a conversion rate of 32 Hz. The low frequency offset, undesired signal modulation caused by the modification of the on-resistance of the transistor switches is pushed to higher frequency by the slow chopping as shown in Fig. 10(a). As shown in Fig. 10(b), the DC offset reduction due to nested chopping is reduced by almost 500 μV with respect to without slow chopping. Tables 1 and 2 shows the specifications of the two types of sensors. The front-end IC is implemented on a single poly, 6-level metal 0.18- μm CMOS process. The differential amplifiers in the integrator has 68.2 dB DC gain and the class AB buffer amplifier for resistor string DAC has 86 dB DC gain. The total power consumption of AFE is 23.4 mW at a supply voltage of 1.8 V for all 16 sensor channels. The chip core area is $2.65 \times 0.95 \text{ mm}^2$. The analog front end IC achieves is 91 dB SNR.

3 Signal denoising

Following the circuit design aspects, this section describes the steps the signal processing and recognition stage. We start by describing signal denoising using wavelets and then continue with the feature extraction and pattern classification approaches.

3.1 Noise in acquired sensor data

Data acquisition is the first step in data analysis; sensors collect the data and convert them into an electrical signal,

which is used for subsequent analysis. However, the electronic interface also introduces noise into the sensor measurements which may result in inaccurate classification of the responses. Amperometric sensors detect analytes using the modulation of current flow caused by the electron transfer reactions of the chemical. The current is a direct measure of the rate of the electron transfer reaction and hence is proportional to the concentration of the analyte [25]. Conductometric sensors rely on the chemical modulation of the conductivity of selected nanostructures by the target analyte. The change in electrical resistance or sensitivity is given by

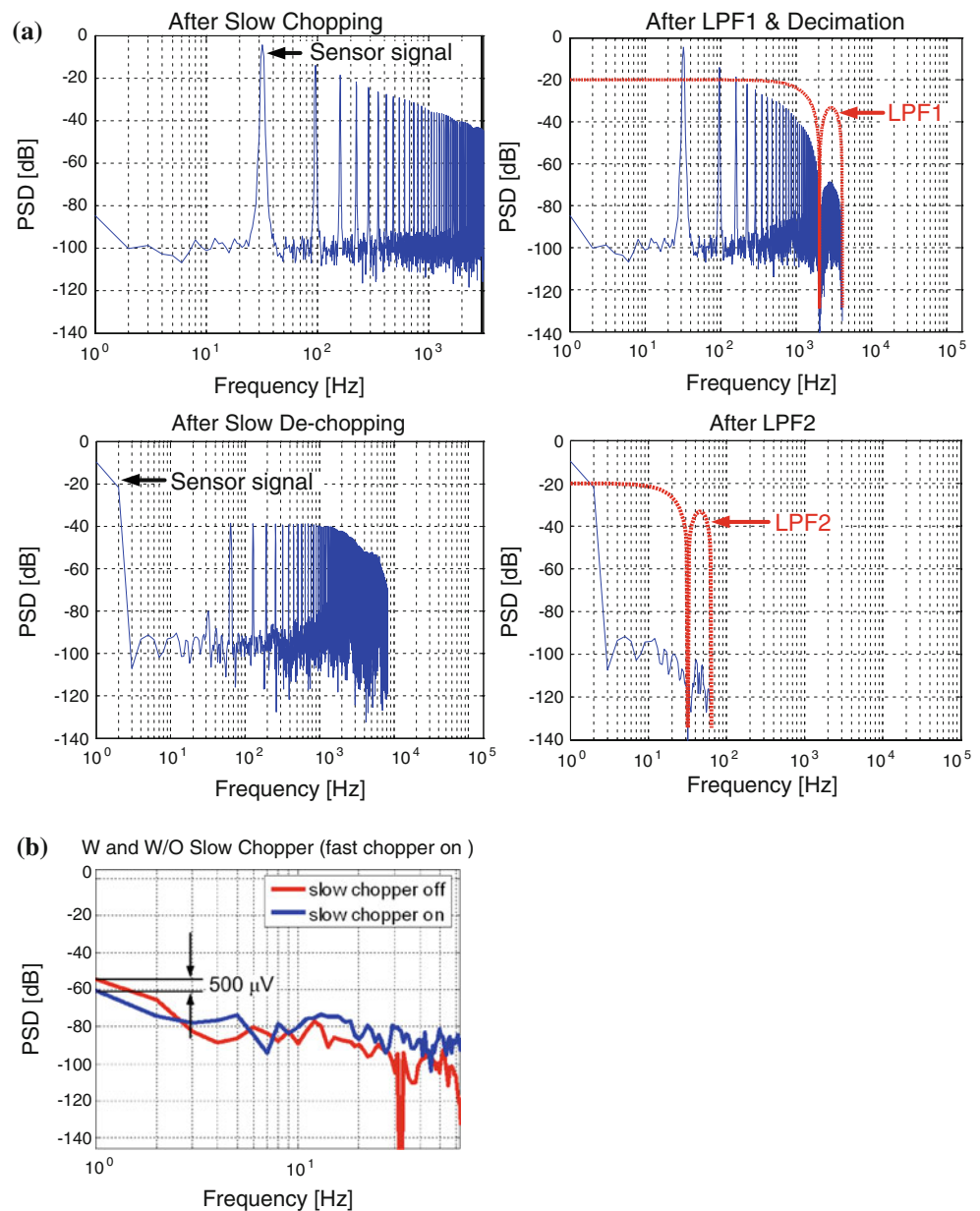
$$S = \frac{R - R_0}{R_0}, \quad (1)$$

where R_0 and R are the original and modified resistances respectively. Ideally, the sensitivity is proportional to the concentration of the analyte. In our case, the current being measured is in the order of nAs and the change in resistance is in the order of $\mu\Omega\text{s}$. Due to the low signal-to-noise (SNR) ratio, the signal peaks, that indicate the presence of analytes, can be easily corrupted. This creates difficulties in measurement of peak parameters such as peak height, width and shape. Hence signal denoising is essential to improve the sensitivity and accuracy of e-noses.

3.2 DWT-based denoising

The Discrete Wavelet Transform (DWT) is a linear transformation that can be used to analyze temporal and spectral properties of non-stationary signals. The DWT of a sequence $x(n)$ is defined by the following equation

Fig. 10 a Measured PSD of the nested chopped $\Sigma\Delta$ ADC at each critical point **b** Offset reduction



$$W(n) = \sum_j \sum_k x(n) 2^{-j/2} \psi(2^{-j}n - k), \quad (2)$$

where $\psi(\cdot)$ is the transforming function referred as the mother wavelet. The DWT decomposes the signal into coarse and fine scales, thereby providing a multi-resolution representation. The DWT is computed by application of successive levels of pairs of analysis filters to the input signal. The advantage of wavelet representation is that it can provide time and frequency parameters for specific dynamic signal events, i.e. *time–frequency localization*. In contrast, the Fourier transform based filtering methods assume that the signal is stationary and thus cannot provide any information on the variations in the spectrum with respect to time.

Wavelet based denoising was originally proposed by Donoho [26]. DWT based denoising techniques for biosensors have been discussed in [27]. Denoising using the DWT is a nonlinear operation that involves the following steps:

- Select or design a suitable wavelet transform on the noisy data to obtain the wavelet coefficients.
- Threshold the wavelet coefficients to remove the noise.
- Zero-pad the signal and take the inverse DWT of the thresholded coefficients from the previous step to interpolate in the time domain and obtain the signal estimate.

Two types of thresholding operations can be performed: hard and soft. In hard thresholding, the wavelet coefficients whose absolute value $|W(n)|$ is less than the specified

Table 1 Specifications of sensor interface

Analog front end IC	
Technology	0.18 μm CMOS, 1 poly 6 metal layers
Die size	2.65 mm \times 0.95 mm
Power consumption	23.4 mW (1.8 V supply)
Opamp spec.	Gain (86 dB), CMRR(95 dB), power(180 μW), GBW(3.4 MHz), PM(67°), CM input(1.6 V), output swing(1.77 V)
Diff. amp spec.	Gain(68.2 dB), CMRR(71 dB), power(190 μW), GBW(3 MHz), PM (90°) CM input range(1.4 V), output swing(3.12 V)
Resistor string DAC	DNL (+0.026/−0.012 LSB)/INL(+0.005/−0.028 LSB), power(402.7 μW with class AB amp)
Current steering DAC	DNL (+0.402/−0.42 LSB)/INL(+0.941/−0.808 LSB), power(93.6 μW)
Slow chopping freq/Fast chopping freq.	32 Hz/131.072 kHz

Table 2 Sensor specifications

Sensor array	
Array size	2 cm \times 2 cm for conductometric sensor 10 cm \times 10 cm for amperometric sensor
Sensor Characteristics	Conductometric sensor: 10 k Ω –10 M Ω Amperometric sensor : 10 nA–100 μA
Electrode spec	Cr/Au (20/180 nm) on SiO ₂ /Si substrates for conductometric sensor, thick carbon film with 1.25 Ag/AgCl for amperometric sensor

threshold limit T_h are set to zero. Soft thresholding, which is used in our simulations, is an extension of hard thresholding; it first performs hard thresholding, and then it reduces the absolute value of the nonzero coefficients by T as shown below.

$$|W(n)| = \begin{cases} 0, & \text{if } |W(n)| \leq T_h \\ |W(n)| - T, & \text{if } |W(n)| > T_h \end{cases} \quad (3)$$

In our simulations, the values of the denoising parameters were determined using a training set drawn from the data. The values which produced the best denoising performance on the training set were assumed to perform similarly on the entire dataset (Fig. 11). The values selected are given below,

- the biorthogonal wavelet achieved the best performance in terms of reduced noise power,
- the level of decomposition was fixed at 7 and
- the threshold T_h was set to be 15.5.

4 Simulations on synthetic data

4.1 Synthetic dataset: motivation

A key problem often associated with sensor signal processing tasks is the lack of relevant and representative data.

The characteristics of signals from different types of chemical sensors vary widely which limits the effectiveness of any generic dataset, even if it were available. The alternative is to wait for the design, fabrication and testing of sensors before embarking on the feature extraction and pattern recognition tasks. But the experiments required to generate the real sensor data can be time-consuming and difficult. However, adopting this approach unnecessarily delays the development of the signal processing module. Hence, the approach followed here is to use synthetic data on which candidate algorithms can be trained and tested. The algorithms are validated against the experimental datasets once they become available.

In this case, typical saturation kinetic equations shown below are used to generate the artificial sensor data.

$$R = \frac{R_{\max} C}{K_s + C}, \quad (4)$$

$$R = \frac{R_{\max} C}{K_s + C + \frac{I_h}{K_i}}, \quad (5)$$

$$R = \frac{R_{\max} C}{K_s + C + \frac{C^2}{K_i}}, \quad (6)$$

where R_{\max} is the saturation response, C represents the analyte concentration and K_i , K_s and I_h are analyte specific constants.

4.2 Simulations on synthetic data

A dataset [28] of synthetically generated sensor responses representing steady-state values was used in the implementation of our customized signal processing modules. The analytes to be identified are ethanol, methane, ammonia and nitrogen-dioxide. The set consists of 36 vectors representing steady-state outputs from 6 sensors, out of which 20 vectors are responses to the 4 single gases (at 5 different concentrations) and the remaining 16 vectors are responses to 4 gas-mixtures (at 4 different concentrations). Thus the

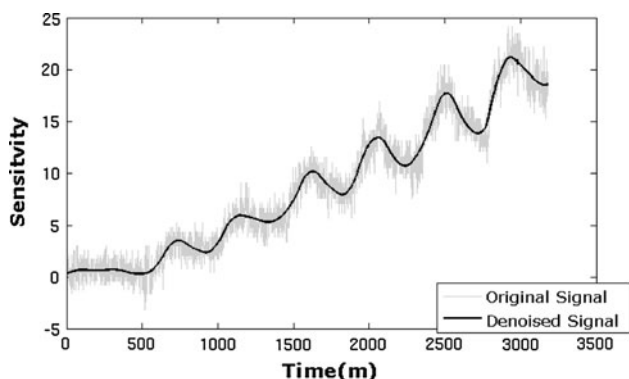


Fig. 11 Original and denoised signals

analytes have to be classified into one of the 8 target classes. A sample plot of concentration versus sensor output for ammonia (NH₃) is shown in Fig. 12.

Principal Component Analysis (PCA) is often used in signal detection, signal compression and dimensionality reduction. It is commonly used in electronic nose applications for feature selection when the sensor outputs are at steady-state. PCA [29] is an approach that derives new and useful features by forming linear combinations of original features. PCA is an orthogonal projection of data from a higher dimensional space to a lower dimensional space such that the variance of the projected data is maximized. Let C be the covariance matrix of a normalized and mean-subtracted dataset X , each row of which is a measurement and W be the matrix of basis vectors. The set of basis vectors is associated with a subset of the eigenvectors of C . The PCA transformation equation is given by

$$Y = XW, \tag{7}$$

Since the eigenvectors are mutually orthogonal, the set of projected data is uncorrelated with each other and as a result,

Fig. 12 Sample calibration plot of hypothetical sensing data from a sensor array for a single gas

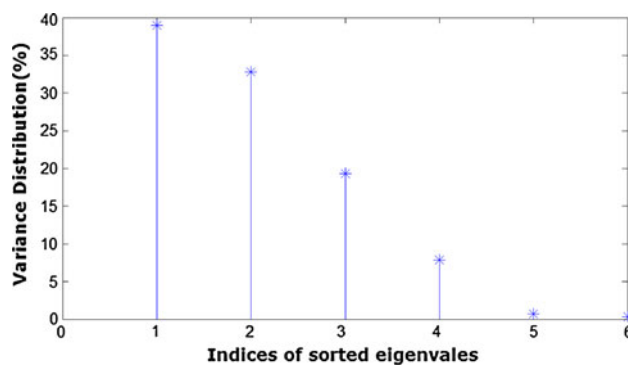
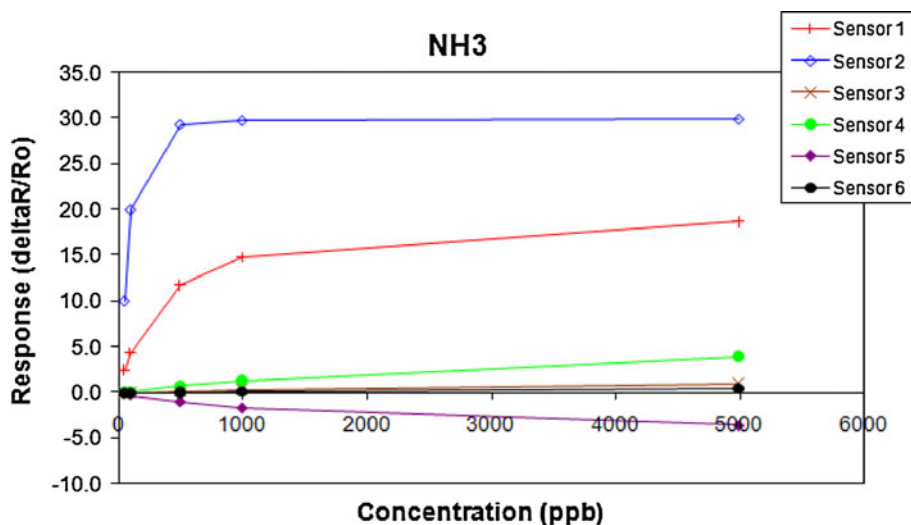
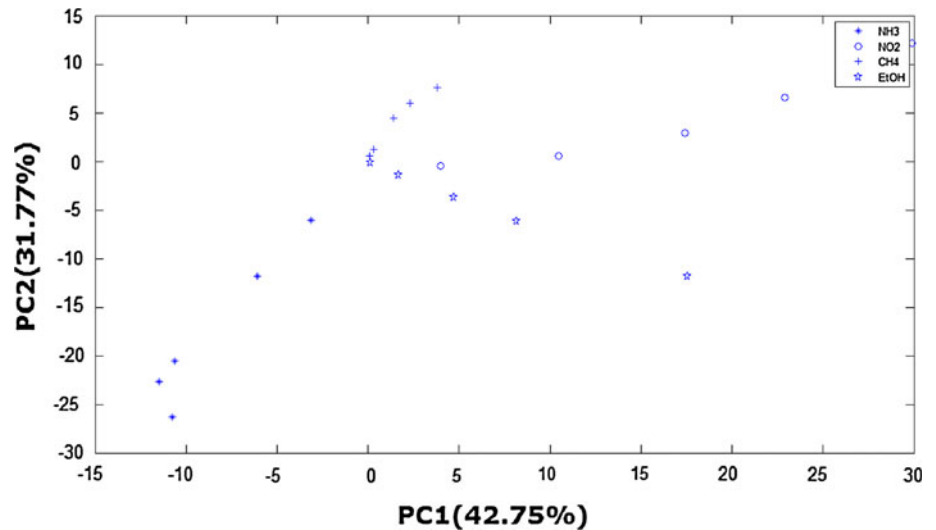


Fig. 13 Distribution of variance among the 6 eigenvalues

each direction accounts for variation which has not been captured by the others. Feature extraction and graphical analysis using PCA has been extensively used in electronic nose applications such as detection of pathogenic bacteria in water [30], distinguishing volatile organic compounds (VOCs) using coated TSM sensors [31].

The projection of the data points representing single gases in the 2-dimensional (Fig. 14) PC space is shown to enable visual analysis. As can be seen, scores representing each gas are clustered together and there is a clear separation between the clusters corresponding to each gas. This motivates the selection of the first few principal vectors as features for the pattern classification algorithms. In this case, the first four principal components account for 95% of the variance as shown in Fig. 13. Thus, we transform the original data by projecting it on the subspace spanned by the four orthogonal eigenvectors corresponding to the four eigenvalues. We adopted the following procedure for training and evaluating the algorithms. A training set was constructed by selecting 25 vectors from the available 36 vectors. The algorithms were trained using only this

Fig. 14 Projection of sensor responses of single gases on the first 2 PC axes



training set. The performance of the trained algorithms was evaluated using the test set, which consisted of the remaining 11 vectors. The training data is used to carry out model selection, i.e. a model that predicts the output (target labels) from the input (sensor responses) with minimum error was chosen. To compensate for the small data set during the training process, n observations were omitted and the rest was used for training (the leave- n out procedure). Classification performance was evaluated using the left-out samples. This procedure was repeated m times, leaving out different sets of n observations during m iterations and averaged the performance (m -fold cross validation) [32]. A value of $m = 5$ and $n = 5$ was used for this simulation.

We customize, implement, and compare the following algorithms that are popular in electronic-nose applications for analyte classification [6]. We provide the details of the pattern classification algorithms used.

- Linear/Quadratic Discriminant Analysis (LDA/QDA) [33]: The aim of discriminant analysis is to find a projection that minimizes distances within classes and maximizes the distances between classes, i.e., it seeks to maximize the ratio of S_b to S_w , where S_b represents the between-group variances and S_w represents the within-group variances.

$$S_b = \sum_{i \in \text{classes}} P_i E |(\mu_i - \mu)(\mu_i - \mu)^T|, \quad (8)$$

$$S_w = \sum_{i \in \text{classes}} P_i E |(x_i - \mu)(x_i - \mu)^T|, \quad (9)$$

where $\{P_i\}_{i=1}^{\text{classes}}$ represents the prior probabilities of the classes, $\{\mu_i\}_{i=1}^{\text{classes}}$ is the mean of the entire data and μ_i

represents the means of the classes. LDA fits a multivariate normal density to each group, assuming that the covariance matrices of all the classes are identical. QDA assumes that the covariance matrices of all the classes are arbitrary. The Discriminant Analysis Toolbox [34] was used for LDA/QDA. For this classifier, we do not perform PCA on the dataset as PCA might ignore the discriminatory features which are used by LDA/QDA for classification.

- Multi-Layer Perceptron (MLP) [32, 35]: MLPs implement linear discriminants but in a space where the inputs have been mapped nonlinearly. To permit a much larger range of decision boundaries the discriminant function $g(x)$ can be expressed as a linear combination of non-linear basis functions ϕ as follows:

$$g(x) = w^T \phi(x) + w_0, \quad (10)$$

where w represents a weight vector whose values are learnt by the MLP using a training algorithm. We used the Netlab toolbox [36] for implementing MLPs. A 2-layer MLP was used in all cases. They were trained using the scaled conjugate gradient (SCG) algorithm, which has modest memory requirements and ensures fast convergence. Weight decay is used to improve generalization. A weight decay parameter of 0.01 and a learning rate parameter of 0.01 were used. The number of neurons in the hidden layer was determined by cross validation.

- Radial Basis Function (RBF) Network [35]: A radial basis function (RBF) network is similar to a MLP, but it achieves pattern classification by fitting each class with a localized kernel function instead of constructing hyperplanes. A RBF network has two layers—namely, a non-linear hidden layer and an output linear layer.

The radial basis function used in our simulations is the Gaussian function,

$$\varphi_k(x) = e^{-\frac{\|x-\mu_k\|^2}{2\sigma_k^2}}, \quad (11)$$

where x is the d dimensional feature vector and μ is the vector determining the centers of the basis functions. This was implemented in MATLAB using Neural Network Toolbox. To determine the weights, the learning rate parameter was fixed at 0.01. As in the previous cases, cross validation was used to determine the number of hidden neurons.

- Learning Vector Quantization (LVQ) [35]: The learning vector quantization (LVQ) network uses supervised competitive learning. Topologically, it consists of a competitive (or unsupervised) hidden layer that learns to classify input vectors and an output linear layer that transforms the competitive layer's outputs into user-defined target classes. The input space is divided into a number of distinct regions called Voronoi cells. For each region, a reconstruction vector (or Voronoi vector) is defined. For a new incoming test vector, its region is first determined, and the data vector is then represented by using the reconstruction vector for that region.

The LVQ1 algorithm was used to perturb the reconstruction vectors so that the quality of the Voronoi cells is improved. The algorithm used for training is LVQ1. The number of hidden neurons was determined by cross-validation. This was implemented using the MATLAB Neural Network Toolbox.

- Support Vector Machines (SVM) [29, 35]: An SVM performs classification by transforming lower-dimensional data into higher dimensional patterns, so that data from two categories can always be separated by a hyperplane. SVMs are known to maximize the separation between the classes, hence they are known as maximum margin classifiers. The vectors that constrain the width of the margin between the classes are the support vectors.

The Spider toolbox [37] was used for implementing SVMs. To extend SVMs to solve multi-class classification problems, one-versus-one (OVO) binary classifiers are constructed to separate one class from another. For a k -class problem, $k(k-1)/2$ binary classifiers are required. The type (polynomial or RBF) of the mapping kernel function and its associated parameter (order and width respectively) was determined by cross validation.

The parameters determined, for the different algorithms, experimentally by cross-validation are given in Table 3. The parameter determined using cross validation for MLPs,

Table 3 Cross validation parameters

Algorithm	Parameter value
MLP	4
RBF	4
LVQ	6
SVM	Polynomial, 2

Table 4 Classification performance on the test set

Algorithm used	Classification (%)	
	Raw data	Extracted features
MLP	54.55	72.73
LDA/QDA	81.82	–
LVQ	72.73	72.73
RBF	81.82	81.82
SVM	72.73	81.82

RBF networks and LVQ networks was the number of neurons in the hidden layer. The type of kernel function (whether polynomial or radial-basis) and its corresponding degree/width were the parameters determined for SVMs. No parameters were selected by cross-validation for LDA/QDA.

For steady-state responses, we train the classifiers using the original dataset and compare their performance to classifiers which are trained on the transformed data set (features extracted using PCA) in order to verify the effectiveness of feature extraction. The results of our simulations are shown in Table 4. The performance columns denote the percentage of correct classifications made on the test dataset. PCA ignores the discriminatory features which are used by discriminant analysis for classification. Hence, we do not perform PCA on the dataset when the classifier is LDA/QDA.

Our results reveal that feature extraction using PCA improves classification. LDA/QDA, RBF and SVM were found to provide the best performance in this scenario on the test set.

5 Simulations with experimental data

5.1 Steady state responses

Three sets of experimental data [38–40] were available for evaluating the steady-state classification performance.

The gases to be identified in Dataset E1 are acetone, ethanol, methanol, dichloromethane (DCM) and methyl ethyl ketone (MEK). The conductometric sensor array used

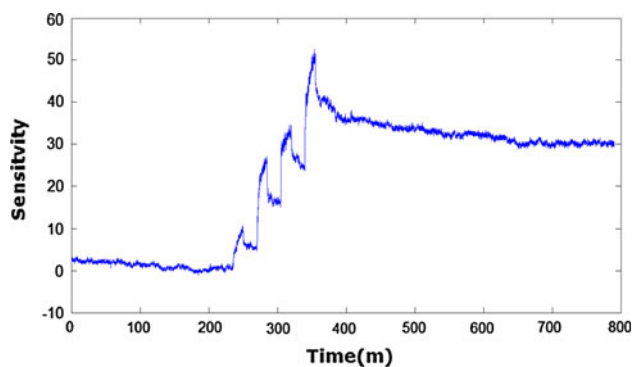


Fig. 15 Sample response of bare SWNT conductometric sensor to acetone

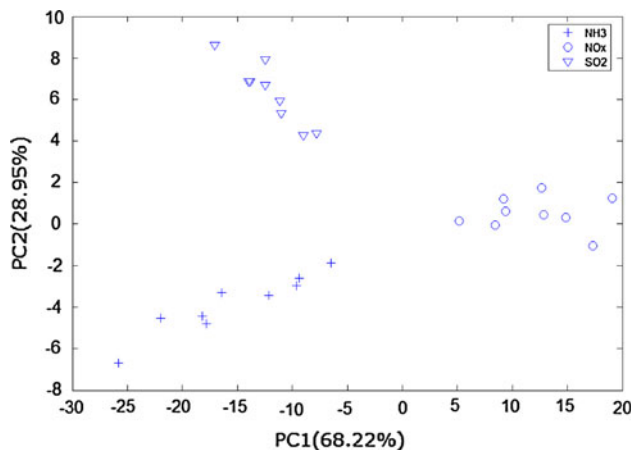
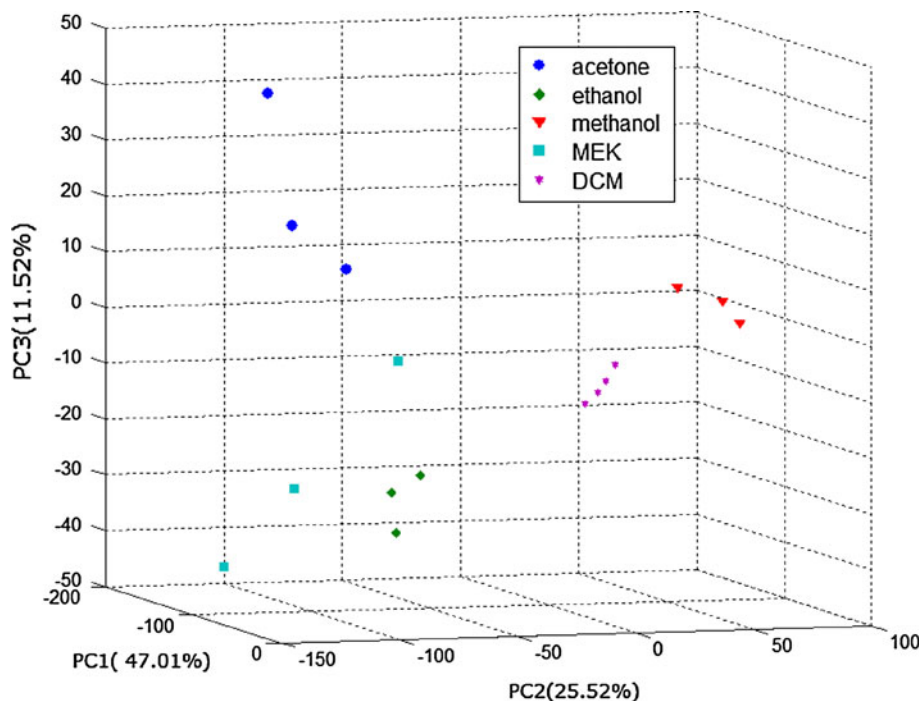


Fig. 16 Dataset E2: projection of sensor responses of single gases on the first 2 PC axes

Fig. 17 Dataset E1: projection of sensor responses of single gases on the first 3 PC axes



for analyte detection consisted of seven sensors: bare, SWNT/OEP, SWNT/TPP, SWNT/Fe-OEP, SWNT/Ru-OEP, SWNT/Fe-TPP and SWNT/Ru-TPP. OEP (octaethyl-porphyrin) and TPP (tetraphenyl-porphyrin) are compounds used to functionalize the sensor surfaces to increase their sensitivity. The sample response of bare SWNT conductometric sensor to acetone is shown in Fig. 15.

The feature data matrix was constructed whose columns were the peak responses from the seven sensors and the rows represent measurements for each gas. For each gas, three measurements (corresponding to 100, 75 and 50% saturation) were selected. Thus, the data matrix had 15 rows and 7 columns. Dataset E2 consisted of responses of three gases: ammonia, sulphur dioxide and nitrogen dioxide to a conductometric array of four sensors: bare, SWNT/Au, SWNT/SnO₂ (as prepared) and SWNT/SnO₂ (annealed). The dimension of the feature data matrix was 27×3 (Fig. 16).

Multivariate analysis was carried out by performing principal component analysis (PCA). In the first case, it was determined that the first three principal components (PCs) accounted for around 88% of the total variance. In the second case, the first two PCs accounted for over 94% of the total variance. As can be seen from Fig. 17, the points are well clustered and were separated with 100% accuracy by all the pattern classification algorithms considered in this work.

It should be noted that in the more challenging problems such as those involving easily confusable gas mixtures (a preliminary dataset consisting of responses to two binary

mixtures was provided in Dataset E3) the clustering will not be as clear as in the cases discussed here. The data points in the mixture dataset were not sufficient to draw conclusions about the suitability of the discussed feature extraction and pattern classification algorithms. We note, however, that a simple linear classifier working on PC features gave a classification accuracy of 87.5% on the training set.

5.2 Transient responses: simulations

Two sets of experimental data [41, 42] were used to evaluate transient responses. The first dataset (Dataset T1) consists of responses of three gases. These are oxygen, nitrofluorene and nitronaphthalene present at the same concentration (10 ppm) detected by four different types of amperometric sensors (C/Pd/Pt/Ru coated WE). The second (Dataset T2) consists of responses of three gases—oxygen, hydrogen sulphide and sulphur-dioxide present at different concentrations (ranging from 400 ppb to 2 ppm) detected by a single amperometric sensor (C coated WE). The sample response of bare C WE amperometric sensor to SO₂ is shown in Fig. 18.

Here, the features based on the transient response are considered. A set of 4 features is extracted from the peaks of the transient signals [43] (Fig. 19). These are:

- (a) the difference between the peak and the baseline,
- (b) the area under the curve,
- (c) the area under the curve left of the peak, and
- (d) the time from the beginning of the signal to the peak.

Cross-validation was used for model selection in this case also. Again, no cross-validation was carried out for discriminant analysis. MLP and LVQ were also tried, but they performed poorly and achieved a classification accuracy of around 50%. The results of the 3 algorithms are

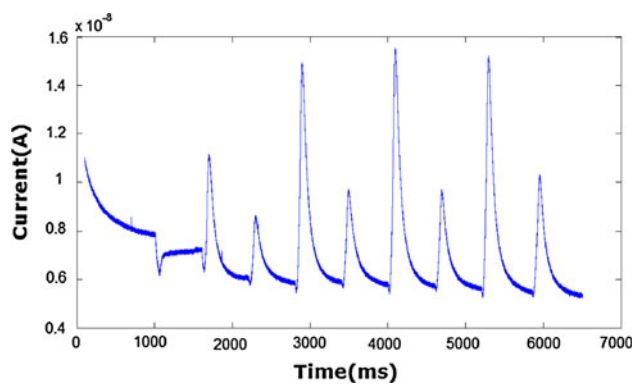


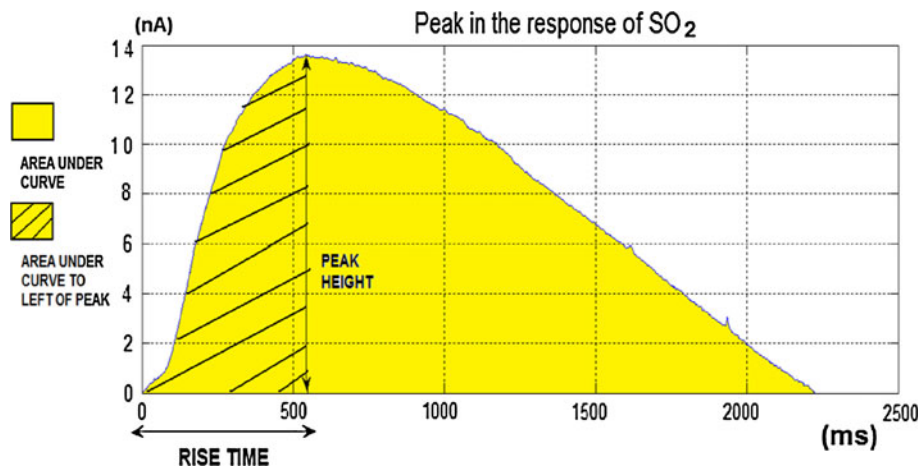
Fig. 18 Sample response of bare C WE amperometric sensor to SO₂

Table 5 Cross validation parameters

Algorithm	Value of parameter
RBF	4
SVM	Polynomial, 2

shown in Table 5. For transient responses, SVMs were found to give the best performance on the test dataset. The performance of the algorithms must be evaluated on larger datasets when they become available before further conclusions can be drawn regarding the discriminative capabilities of the classifiers. Also, the performance of the algorithms was better on the experimental dataset as compared to the synthetic dataset because the latter dataset was more complex—it had 36 records drawn from nine classes (which included single gases and gas mixtures) whereas the former had the same number of records, but drawn from only three classes.

Fig. 19 Transient signal features



6 Conclusions

A signal processing approach was developed for detecting environmental pollutants along with a 0.18- μm CMOS AFE IC designed for a 16 channel gas sensors array. The AFE IC consists of an integrated potentiostat, a low noise I/V converter, a current steering DAC, resistor string DACs and the first-order $\Sigma\Delta$ ADC for both conductometric and amperometric sensors. To reduce offset and residual noise at low frequency that arises due to clock feed through mismatches and integrator mismatches, the chopper stabilization was used.

Following the data acquisition section, the motivation for the feature extraction techniques chosen for steady state and transient responses was provided and the effectiveness of these features with respect to signal classification was analyzed. Techniques to deal with the paucity of training data were also described. For steady-state responses, PCA could be used for feature extraction. For transient responses, the four parameters from the peak of the transient curve were found to provide good features. LDA/QDA and SVMs have shown good performance among the classification algorithms used in this work. We are currently working on larger datasets to verify and test further the performance of the classifiers. Future directions to this work include developing techniques to determine the concentration of the analytes when they are present in mixtures.

Acknowledgment This work was supported through the NIH Genes, Environment and Health Initiative through award 3U01ES016026-02S1.

References

1. Reed, M. D., et al. (2008). Health effects of subchronic inhalation exposure to gasoline engine exhaust. *Inhalation Toxicology*, 20(13), 1125–1143.
2. U.S. EPA. (2002). Health assessment document for diesel engine exhaust (Final 2002). U.S. Environmental Protection Agency, Office of Research and Development, National Center for Environmental Assessment, Washington Office, Washington, DC, EPA/600/8-90/057F.
3. Sydbom, A., et al. (2001). Health effects of diesel exhaust emissions. *European Respiratory Journal*, 17, 733–746.
4. Bhatia, R., Lopipero, P., & Smith, A. H. (1998). Diesel exhaust exposure and lung cancer. *Epidemiology*, 9(1), 84–91.
5. Office of population genomics. Available online at <http://www.genome.gov/>.
6. Scott, S. M., James, D., & Ali, Z. (2007). Data analysis for electronic nose systems. *Microchimica Acta*, 156(3–4), 183–207.
7. Gardner J. W., & Bartlett P. N. (1999). Electronic noses: Principles and applications. Oxford University Press, USA.
8. Olafsdottir, G., Jonsdottir, R., Lauzon, H. L., Luten, J. B., & Kristbergsson, K. (2005). Characterization of volatile compounds in chilled cod (*Gadus morhua*) fillets by gas chromatography and detection of quality indicators by an electronic nose. *Journal of Agricultural and Food Chemistry*, 53(26), 10140–10147.
9. Marina, S., et al. (2007). Use of a MS-electronic nose for prediction of early fungal spoilage of bakery products. *International Journal of Food Microbiology*, 114(1), 10–16.
10. Di Natale, C., et al. (1999). Electronic nose analysis of urine samples containing blood. *Physiological Measurement*, 20, 377–384.
11. Shykhon, M. E., Morgan, D. W., Dutta, R., Hines, E. L., & Gardner, J. W. (2004). Clinical evaluation of the electronic nose in the diagnosis of ear, nose and throat infection: a preliminary study. *Journal of Laryngology and Otolaryngology*, 118, 706–709.
12. Engin, G. (1997). Characterization of sewage and sewage odors by using an electronic nose. Master's Thesis, Department of Civil Engineering, University of Hertfordshire, U.K.
13. Rock, F., Barsan, N., & Weimar, U. (2008). Electronic nose: Current status and future trends. *Chemical Reviews*, 108(2), 705–725.
14. Zhou, H., Homer, M. L., Shevade, A. V., & Ryan, M. A. (2006). Nonlinear least-squares based method for identifying and quantifying single and mixed contaminants in air with an electronic nose. *IEEE Sensors Journal*, 6, 1–18.
15. Blaschke, M., et al. (2006). MEMS gas-sensor array for monitoring the perceived car-cabin air quality. *IEEE Sensors Journal*, 6(5), 1298–1308.
16. Nicolas, J., Romain, A. C., & Ledent, C. R. (2006). The electronic nose as a warning device of the odour emergence in a compost hall. *Sensors and Actuators B*, 116(1–2), 95–99.
17. Mulchandani, A., Myung, N. V., Deshusses, M. A., Cocker, D., Wang, J., Bakkaloglu, B., et al. (2008). Nanosensor array for real-time monitoring of diesel and gasoline exhaust exposure. *Epidemiology*, 19(6), S62.
18. Konnanath, B., Kim, H., Spanias, A., Bakkaloglu, B., Wang, J., Mulchandani, A., & Myung, N. (2009). A real-time monitoring system for diesel and gasoline exhaust exposure. In *Proceedings of the IEEE 16th International Conference on DSP*, pp. 1–5, Jul 2009.
19. Wang, J. (1985). *Stripping analysis: Principles, instrumentation, and applications*. VCH: Deerfield Beach.
20. Martin, S. M., Gebara, F. H., Strong, T. D., & Brown, R. B. (2004). A low-voltage chemical sensor interface for systems-on-chip: The fully-differential potentiostat. In *Proceedings of the IEEE International Symposium on Circuits and Systems*, vol. 4, pp. 892–895.
21. Castello, R., & Gray, P. R. (1985). A high-performance micro-power switched-capacitor filters. *The IEEE Journal of Solid-State Circuits*, SC-20(6), 1122–1132.
22. Zhang, T., Mubeen, S., Myung, N., & Deshusses, M. A. (2008). Recent progress in carbon nanotube-based gas sensor. *Nanotechnology*, IOP, pp. 1–14.
23. Bakker, A., Thiele, K., & Huijsing, J. H. (2000). A CMOS nested-chopper instrumentation amplifier with 100-nV offset. *The IEEE Journal of Solid-State Circuits*, 35(12), 1877–1883.
24. Wonseok Oh, Bakkaloglu, B., Wang, C., & Hoon, S. K. (2008). A CMOS low noise, chopper stabilized low-dropout regulator with current-mode feedback error amplifier. *IEEE Transactions on Circuits and Systems*, 55(10), Nov 2008.

25. Wang, J. (1996). Electrochemical transduction. In R. F. Taylor & J. S. Schultz (Eds.), *Handbook of chemical and biological sensors* (pp. 123–137). Bristol, UK: IOP Publishing.
26. Donoho, D. L. (1995). De-noising by soft thresholding. *IEEE Transactions on Information Theory*, 41(3), 613–627.
27. Jagtiani, A. V., Sawant, R., Carletta, J., & Zhe, J. (2008). Wavelet transform-based methods for denoising of Coulter counter signals. *Measurement Science and Technology*, 19(6), 1–15.
28. Deshusses, M. (2008). Dataset-S: Synthetic dataset, Department of Chemical and Environmental Engineering, University of California-Riverside.
29. Duda, R. O. (2006). *Pattern recognition for machine learning*. Berlin: Springer.
30. Gardner, J. W., Shin, H. W., Hines, E. L., & Dow, C. S. (2000). An electronic nose system for monitoring the quality of potable water. *Sensors and Actuators B*, 69(3), 336–341.
31. Barko, G., & Hlavay, J. (2000). Application of principal component analysis for the characterization of a piezoelectric sensors array. *Analytica Chimica Acta*, 367(1–3), 135–143.
32. Ripley, B. D. (1996). *Pattern recognition and neural networks*. Cambridge: Cambridge University Press.
33. Duda, R. O., Hart, P. E., & Stork, D. G. (2001). *Pattern classification*. New York: Wiley.
34. Discriminant analysis toolbox. Available online at <http://www.mathworks.com/matlabcentral/fileexchange/authors/1714>.
35. Haykin, S. (1999). *Neural networks: A comprehensive foundation*. New Jersey: Prentice Hall.
36. Netlab neural network software. Available online at <http://www.ncrg.aston.ac.uk/netlab/index.php>.
37. The Spider version 1.71 for MATLAB. Available online at <http://www.kyb.mpg.de/bs/people/spider/main.html>.
38. Mulchandani, A. et al. (2009). Dataset-E1: Experimental dataset, Department of Chemical and Environmental Engineering, University of California-Riverside.
39. Mulchandani, A. et al. (2009). Dataset-E2: Experimental dataset, Department of Chemical and Environmental Engineering, University of California-Riverside.
40. Wang, J., et al. (2009). *Dataset E3: Experimental dataset*. University of California-San Diego: Laboratory for Nanobioelectronics.
41. Wang, J., et al. (2008). Dataset T1: Experimental dataset, Center for Bioelectronics and Biosensors, Arizona State University.
42. Wang, J., et al. (2008). *Dataset T2: Experimental dataset, Laboratory for Nanobioelectronics*. San Diego: University of California.
43. Haddad, R., Carmel, L., & Harel, D. (2007). A feature extraction algorithm for multi-peak signals in electronic noses. *Sensors and Actuators B*, 120(2), 467–472.
44. Bard, A. J., & Faulkner, L. R. (2001). *Electrochemical methods: Fundamentals and applications*. New York: Wiley.
45. Levine, P. M., Gong, P., Levicky, R., & Shepard, K. L. (2008). Active CMOS sensor array for electrochemical biomolecular detection. *The IEEE Journal of Solid-State Circuits*, 43(8), 1859–1871.
46. Malcovati, P., Brigati, S., Francesconi, F., Maloberti, F., Cusinato, P., & Baschiroto, A. (2003). Behavioral modeling of switched-capacitor sigma-delta modulators. *IEEE Transactions on Circuit and System*, 50(3), 352–364.
47. Schreier, R., & Temes, G. C. (2005). *Understanding delta-sigma data converters*. Hoboken, NJ: IEEE Press, Wiley-Interscience.
48. Martin, S. M., Gebara, F. H., Larivee, B. J., & Brown, R. B. (2004). A CMOS integrated microinstrument for trace detection of heavy metals. In *Proceedings of the IEEE International Symposium on Circuits and Systems*, vol. 4, pp. 892–895.



Hyuntae Kim received the B.S. and M.S. degrees in Electronics Engineering from Soongsil University, Seoul, Korea, in 1999 and 2001 respectively. He is currently working toward the Ph.D. degree in Electrical Engineering at Arizona State University. His research interests include biosensors, sensor interface circuitry, sigma-delta ADC and biomedical and instrumentation circuits and systems.



Bharatan Konnanath received the B.E. degree in Electronics and Communication Engineering from the University of Madras, Chennai, India, in 2004 and the M.S. degree in Electrical Engineering from Arizona State University, Tempe, USA, in 2009 where he is currently a Research Technician in the Department of Electrical Engineering. His research interests are in the areas of sensor signal processing, pattern recognition and audio/video signal process-

ing and coding.



Prasanna Sattigeri is a PhD student at Arizona State University. He received his B.Tech (Hons) in Electrical Engineering from the National Institute of Technology, Jamshedpur, India in 2008. His research interests lie in Machine Learning and its broad applications with focus on use of non-parametric Bayesian methods in image/video segmentation and sensor signal classification.



Joseph Wang received his PhD from the Israel Institute of Technology in 1978. From 1978 to 1980 he served as a research associate at the University of Wisconsin (Madison) and joined New Mexico State University (NMSU) in 1980. In 2001–2004 he held a Regents Professorship and a Manasse Chair position at NMSU, and from 2004 to 2008 he served as the director of the Center for Bioelectronics and Biosensors of Arizona State University (ASU). Currently, he is Professor in the Department of Nanoengineering at the University of California, San Diego (UCSD). Professor

Wang has published more than 760 papers and holds 12 patents. He became the most cited electrochemist in the world in 1996 and was ranked in the 2nd place in the ISI list of Most Cited Researchers in Chemistry in 1997–2007. Professor Wang is the Editor-in-Chief of *Electroanalysis*. His scientific interests are concentrated in the areas of nanomachines, bioelectronics, bionanotechnology and electroanalytical chemistry.



Ashok Mulchandani is a Professor in the Department of Chemical and Environmental Engineering at the University of California and Fellow of the American Association for Advancement of Science. Prof. Mulchandani is the Editor-in-Chief of the *Applied Biochemistry and Biotechnology* journal. He has received several honors and awards including Research Initiation Award from the national Science Foundation and Faculty Participation Award

from the Department of Energy. Prof. Mulchandani's research is focused on the application of Nanotechnology and Biotechnology for the creation of (bio)analytical devices, novel (bio)remediation technologies and nanostructured materials. He has published over 160 peer-reviewed journal publications, 11 book chapters, 12 conference proceedings articles and over 175 conference abstracts. He has co-edited four textbooks that include very popular *Enzyme and Microbial Biosensors: Protocols and Techniques* and *Affinity Biosensors: Protocol and Techniques*.



Nosang Myung received his B.S. M.S. and Ph. D. Degree in Chemical Engineering from the University of California, Los Angeles in 1994, 1997, and 1998, respectively. He spent 3 years as a research engineer at the same institution. In 2001–2003, he joined micro electromechanical systems (MEMS) group at Jet Propulsion Laboratory (JPL) which is one of NASA center as a member of engineering staff. Currently, he is an associate professor in

Department of Chemical and Environmental Engineering at University of California, Riverside. During his career, he received a few awards including University of California Regent Fellowship, Jet Propulsion Laboratory Spot Award, Abner Brenner gold medal award from American Electroplaters and Surface Finishers Society (AESF). Dr. Myung's research interests are focused on the synthesis of nano-engineered materials and apply these materials in various advanced applications including spintronics, sensors, electronics, optoelectronics, energy harvesting, and environmental remediation. Currently, he published 102 peer-reviewed journal papers, one US patent, three filed patent applications.



Marc A. Deshusses is Professor in the Dept. of Civil and Environmental Engineering at Duke University and Fellow of the American Association for Advancement of Science. He received his B.S., M.S., and Ph.D. at Swiss Federal Institute of technology. His broad research interests are related to the design, analysis and application of processes for the bioremediation of contaminated air, water and soils. Current focus is bioreactors for air and

groundwater pollution control, and the development of gas-phase sensors based on functionalized nanomaterials. Research interests include biomolecular techniques for monitoring microorganisms in complex mixed cultures, bioenergy, biofilms, indoor air quality, nanomaterials for environmental remediation and mathematical modeling of environmental bioprocesses.



Andreas Spanias is Professor in the School of Electrical, Computer, and Energy Engineering at Arizona State University (ASU). He is also the founder and director of the SenSIP industry consortium. His research interests are in the areas of adaptive signal processing, speech processing, and audio sensing. He and his student team developed the computer simulation software Java-DSP (J-DSP—ISBN 0-9724984-0-0). He is author of two text books: *Audio Processing and Coding by Wiley and DSP; An Interactive Approach*. He served as Associate Editor of the *IEEE Transactions on Signal Processing* and as General Co-chair of IEEE ICASSP-99. He also served as the IEEE Signal Processing Vice-President for Conferences. Andreas Spanias is co-recipient of the 2002 IEEE Donald G. Fink paper prize award and was elected Fellow of the IEEE in 2003. He served as distinguished lecturer for the IEEE Signal processing society in 2004.

ing and Coding by Wiley and DSP; An Interactive Approach. He served as Associate Editor of the *IEEE Transactions on Signal Processing* and as General Co-chair of IEEE ICASSP-99. He also served as the IEEE Signal Processing Vice-President for Conferences. Andreas Spanias is co-recipient of the 2002 IEEE Donald G. Fink paper prize award and was elected Fellow of the IEEE in 2003. He served as distinguished lecturer for the IEEE Signal processing society in 2004.



Bertan Bakkaloglu joined the ASU faculty in August 2004. Prior to joining ASU, he worked at Texas Instruments and was responsible for analog, mixed signal and RF system-on-chip development for wireless and wireline communication transceivers. He is a technical committee member for IEEE Radio Frequency Integrated Circuits Conference and founding chair of the IEEE Solid State Circuits Society Phoenix Chapter.